RESEARCH ARTICLE

NANO · MICRO small
www.small-journal.com

Stable Zinc Electrode Reaction Enabled by Combined Cationic and Anionic Electrolyte Additives for Non-Flow Aqueous Zn—Br_2 Batteries

*Jeonghyun Kim, Hyeonghun Park, Youngin Cho, Taegyoung Lee, Hyerim Kim, Chanho Pak, Hyeong-Jin Kim, and Sangryun Kim**

Aqueous zinc–bromine batteries hold immense promise for large-scale energy storage systems due to their inherent safety and high energy density. However, achieving a reliable zinc metal electrode reaction is challenging because zinc metal in the aqueous electrolyte inevitably leads to dendrite growth and related side reactions, resulting in rapid capacity fading. Here, it is reported that combined cationic and anionic additives in the electrolytes using $CeCl_3$ can simultaneously address the multiple chronic issues of the zinc metal electrode. Trivalent Ce^{3+} forms an electrostatic shielding layer to prevent Zn^{2+} from concentrating at zinc metal protrusions, while the high electron-donating nature of Cl^- mitigates H_2O decomposition on the zinc metal surface by reducing the interaction between Zn^{2+} and H_2O. These combined cationic and anionic effects significantly enhance the reversibility of the zinc metal reaction, allowing the non-flow aqueous Zn—Br_2 full-cell to reliably cycle with exceptionally high capacity (>400 mAh after 5000 cycles) even in a large-scale battery configuration of 15 × 15 cm^2.

1. Introduction

Currently, grid-scale energy storage systems (ESS) are predominantly dominated by lithium-ion batteries that utilize organic solvent-based electrolytes.[1] Despite their superior energy storage performance, lithium-ion batteries still possess inherent drawbacks, including safety concerns, high material costs, and uneven distribution of raw materials. This has spurred the exploration of alternative energy storage systems based on aqueous rechargeable batteries.[2] In particular, increasing safety concerns regarding the use of conventional lithium-ion batteries with flammable organic liquid electrolytes in ESS have accelerated research into various types of aqueous batteries.

The combination of redox materials plays a crucial role in aqueous batteries, as their energy density and stability significantly influence battery performance. In this context, aqueous Zn—Br_2 batteries that utilize redox reactions of Zn and Br at the anode and cathode, respectively, emerge as among the most prominent candidates owing to their high theoretical energy density (>400 Wh kg^{-1}),[3] power density (>100 mW cm^{-2})[3], and low active material costs (5–8 \$ kWh^{-1}):[4] 1) In detail, Zn metal provides the highest volumetric energy density (5885 mAh cm^{-3})[5] among known anode materials. 2) Zn metal is also naturally abundant and is (electro)chemically compatible with the aqueous electrolyte system.[6] 3) In addition, bromine (Br) exhibits high specific capacity (200 Ah L^{-1}),[5] high redox potential (1.07 V vs standard hydrogen electrode (SHE)),[7] and superior water stability.[5] Based on these conspicuous advantages, various types of aqueous Zn—Br_2 batteries such as redox flow,[8] membrane-free,[3,9] and non-flow[3,10] types have been introduced to realize the high-performance aqueous battery systems.

However, achieving reliable operation of aqueous Zn—Br_2 batteries with stable cycling capabilities is nontrivial. One of the inherent challenges is dendritic growth and related parasitic side reactions of the zinc metal anode upon cycling.[11] It is well-known that zinc metal anode is prone to dendrite growth during plating, and these changes are repeated and accelerated over cycling, leading to internal short circuits and dead Zn. In addition, the redox reactions of Zn in the aqueous environment are inevitably accompanied by unwanted water-derived side reactions, namely the hydrogen evolution reaction (HER).[12] Several strategies have been employed to address these issues, such as surface coating,[13] zinc metal engineering,[14] and electrolyte additives.[15] However, ensuring stable Zn reactions for prolonged cycling, especially at high areal current densities, remains a challenge. More difficultly, as the reaction of the zinc metal anode in aqueous Zn—Br_2 batteries starts from Zn^{2+} existing in the electrolyte, the aforementioned Zn-derived side reactions

J. Kim, H. Park, Y. Cho, T. Lee, H. Kim, C. Pak, H.-J. Kim, S. Kim
Graduate School of Energy Convergence
Institute of Integrated Technology
Gwangju Institute of Science and Technology (GIST)
123 Cheomdangwagi-ro, Buk-gu, Gwangju 61005, Republic of Korea
E-mail: sangryun@gist.ac.kr

The ORCID identification number(s) for the author(s) of this article can be found under https://doi.org/10.1002/smll.202401916

DOI: 10.1002/smll.202401916

are inter-influenced by those of Br^- in the cathode side, causing additional side reactions such as generation of Br_2 gas and the formation of polybromide anions (Br_3^-, Br_5^-, Br_7^-, etc.).[16] For these reasons, in most cases, the performance degradation of aqueous Zn—Br_2 batteries is more severe than that of conventional Zn aqueous ones.

In an effort to stabilize the zinc metal anode reactions in aqueous Zn—Br_2 batteries, herein, we report a new approach of simultaneously engaging cationic and anionic additives, namely cerium cation (Ce^{3+}) and chloride anion (Cl^-) ($CeCl_3$ as a compound), in the aqueous electrolyte. The trivalent Ce^{3+} improves the reversibility of Zn plating/stripping by forming an electrostatic shielding layer that prevents the concentration of zinc ions. Moreover, the high electron-donating nature of Cl^- mitigates the HER on the surface of the zinc metal anode by weakening the interaction between Zn^{2+} and H_2O. On the basis of these combined cationic and anionic effects, in the case of large-area (15×15 cm^2) cell configurations, non-flow aqueous Zn—Br_2 batteries with the $CeCl_3$ additive exhibit superior cycling stability (>400 mAh after 5000 cycles) at a high current density of 20 mA cm^{-2}. This research provides a promising guideline toward practical large-scale aqueous Zn—Br_2 batteries, marking a significant milestone in advanced energy storage solutions.

In contrast to previous studies relying on single-type additives, our approach offers a distinctive approach to stabilize the zinc metal anode. This study contributes to advancing the understanding of electrode stabilization strategies in aqueous battery systems. Furthermore, the insights gained from this research hold significant implications for the development of high-performance and reliable energy storage technologies for diverse applications.

2. Results and Discussion

2.1. Electrochemical Test of a Graphite (Cathode)/Zn (Anode) Cell

Figure 1a illustrates the schematic diagrams of synthetic routes for the pristine electrolyte and the modified electrolyte containing $CeCl_3$. The electrolytes were prepared by simply mixing $ZnBr_2$ salt, $CeCl_3$ additive, and deionized (DI) water (See the Experimental Section for details). The optical photographs display that both electrolytes are transparent with no visible differences, indicating that the synthesized electrolytes are homogeneously dispersed (Figure S1, Supporting Information).

The non-flow graphite (cathode)/Zn (anode) cells (Figure 1b; Figure S2a, Supporting Information) using the modified electrolytes exhibited superior electrochemical properties in various aspects, such as cycle life, coulombic efficiency (CE), energy efficiency (EE), and rate capability. From the testing of various concentrations of $CeCl_3$ (Figure S3, Supporting Information), 0.03 M was chosen as the main modified electrolyte for the current investigation. When galvanostatically cycled at a charging current density of 20 mA cm^{-2} with an areal capacity of 2 mAh cm^{-2} and at a discharging current density of 20 mA cm^{-2} (cut-off voltage: 0.01 V), the cells with the pristine and modified electrolytes display very similar profiles during the first cycle (Figure S4, Supporting Information). The discharge capacities of the modified electrolyte and pristine electrolyte cells were 7.171 mAh and 7.231 mAh, respectively.

After the initial cycle, however, both cells present different behaviors during prolonged cycling (Figure 1c,d). The average CEs and EEs of the modified and pristine electrolyte cells during 500 cycles were 97.8%, 68.4%, and 89.8%, 63.1%, respectively (Figure 1e–g). These results clarify that $CeCl_3$ significantly enhances the reversibility of aqueous Zn—Br_2 batteries.

Moreover, as shown in the dQ/dV plots (Figure 1h; Figure S5, Supporting Information), the modified electrolyte cell exhibits lowered overpotential, which implies that the $CeCl_3$ additive contributes to the mitigation of reaction resistance. The decreased resistance was also verified by electrochemical impedance spectroscopy (EIS) analyses (Figure S6, Supporting Information). Therefore, the higher EE of the modified electrolyte cell is ascribed to its improved CE and lowered battery resistance. In contrast, most of the previous approaches involving other electrolyte additives to stabilize zinc metal reactions impair zinc ion migration and consequently sacrifice the intrinsic electrochemical performance of the electrolyte.[17]

The modified electrolyte cell also displays improved rate capability. Figure 1i shows the CEs at different discharging current densities (5, 10, 20, 40, 60, and 80 mA cm^{-2}) with a fixed charging current density of 20 mA cm^{-2} after 10 cycles of activation. The cell with the modified electrolyte exhibits higher CEs under all discharging current densities. The reduction of overpotential by the $CeCl_3$ additive is also observed at high discharging current densities (Figure S7, Supporting Information). These excellent performances of the modified electrolyte cells are attributed to the combined contributions of Ce^{3+} and Cl^- additives in the electrolyte to the enhanced stability of the zinc electrode during cycling. This is well reflected in the reversibility of the zinc electrode reaction, as discussed in the next section.

2.2. Analysis of Zinc Surface and Bulk Electrolyte

The electrochemical processes of the modified electrolyte cell were further investigated by various analyses. Cyclic voltammetry (CV) tests using both electrolytes indicate that the $CeCl_3$ additive has almost no effect on the Br_2/Br^- reaction at the cathode (Figures S8,S9, Supporting Information). In addition, Raman spectroscopy analyses after cycling detect no by-products (such as Br_2Cl^- and Br_4Cl^-)[18] by the interaction between the Br_2 cathode and the $CeCl_3$ additive (Figure S10, Supporting Information). Therefore, our additional characterizations focus on the zinc metal anode.

Dendrite formation is one of the critical challenges that must be addressed for the practical application of batteries using metal electrodes. It is well-known that the protrusions of the zinc metal anode generate a stronger electric field compared to the smooth regions.[19] This electric field difference causes the flow of Zn^{2+} to concentrate around the protrusions, ultimately leading to dendrite formation. In fact, our pristine electrolyte cell presented a drastic decrease and increase in the CEs during cycling (Figure 1e), which are caused by the dendrite growth of zinc ions and their recovery.[20]

X-ray photoelectron spectroscopy (XPS) analyses on the zinc metal anode surface after the deposition of Zn^{2+} present only the Zn 2*p* peaks (**Figure 2a,b**). X-ray diffraction (XRD) measurements of the zinc metal anode before and after cycling also confirm only

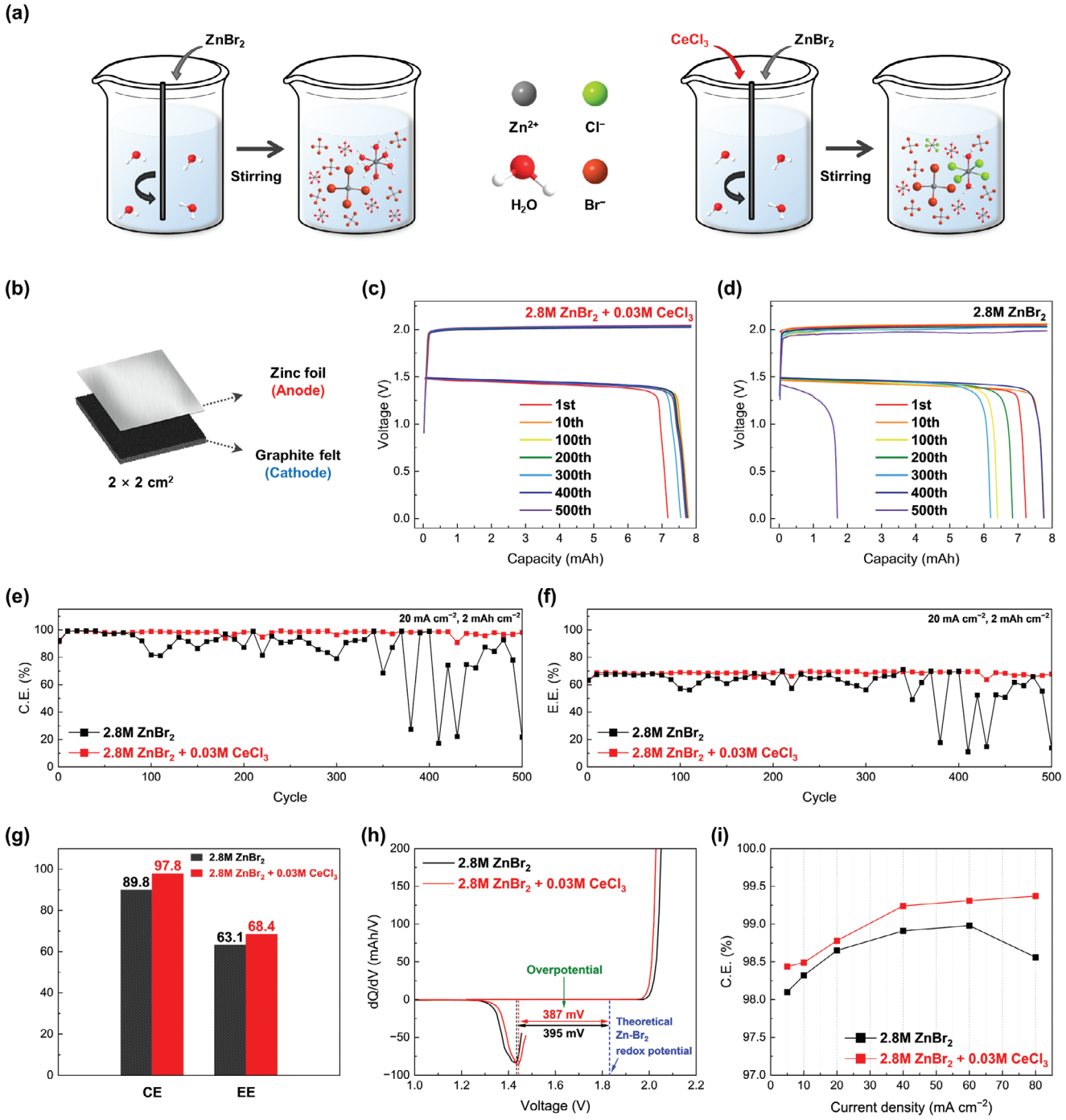

Figure 1. a) Schematic diagrams of synthesis routes of electrolytes, left: pristine electrolyte, right: modified electrolyte. No BCA was used. b) Schematic illustration of the graphite (cathode)/Zn (anode) cell. Charge–discharge profiles of the c) modified electrolyte and d) pristine electrolyte cells. Cycle performances of e) coulombic efficiency and f) energy efficiency. g) Average coulombic efficiencies and energy efficiencies during 500 cycles. h) dQ/dV plots derived from tenth charge–discharge profiles in Figure 1c,d. i) Coulombic efficiency as a function of discharging current density.

the peaks from zinc metal (Figure S11, Supporting Information). In addition, no bonding peaks related to Ce^{3+} were observed in the modified electrolyte from the Raman spectroscopy measurements (Figure S12, Supporting Information). These results reveal that Ce^{3+} exists in the state of free ions in the electrolyte during cycling. Therefore, Ce^{3+}, which has a standard reduction potential (−2.48 V vs SHE) lower than that of Zn^{2+} (−0.76 V vs SHE) and possesses a higher valency than Zn^{2+}, plays a role in inhibiting dendrite formation through the following mechanism; Ce^{3+} approaches near the protrusions of the zinc metal anode, forming an electrostatic shielding layer. This layer can induce the uniform deposition of zinc by exerting

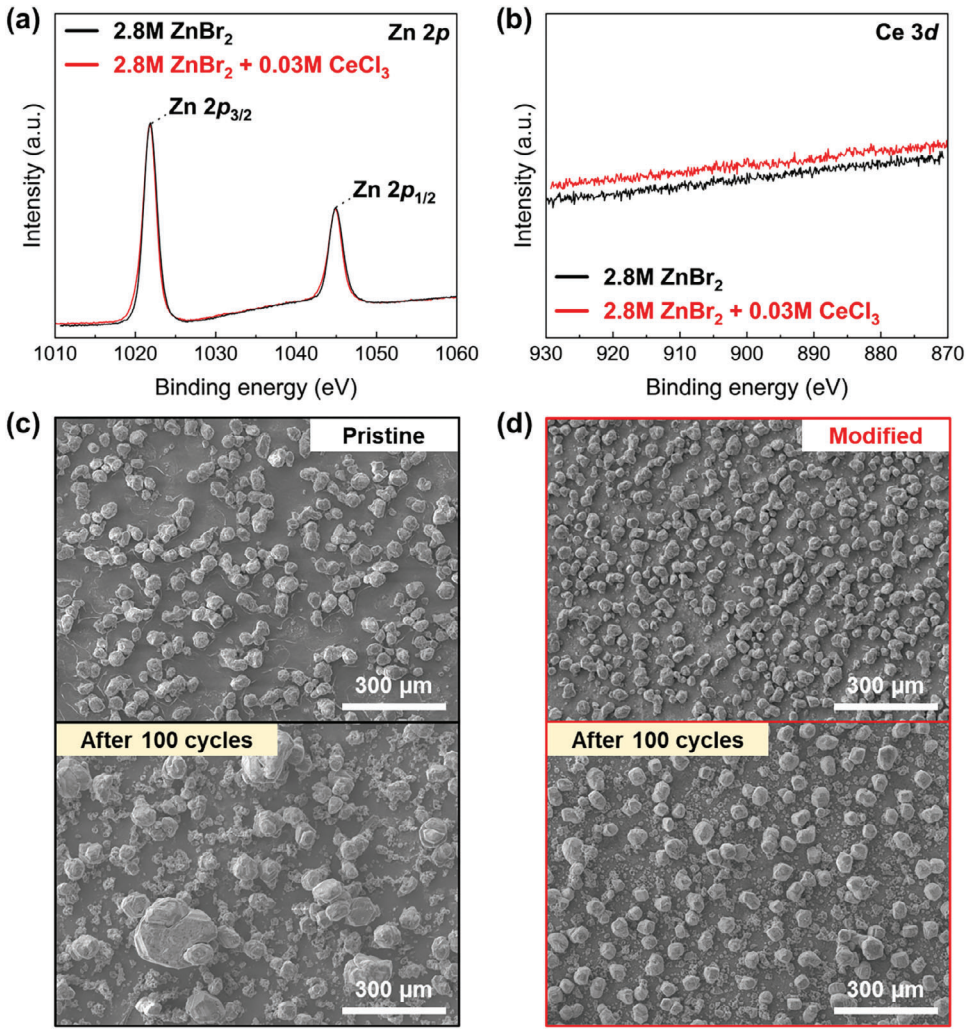

Figure 2. XPS spectra of a) Zn 2*p* and b) Ce 3*d* for the zinc metal anodes after the Zn^{2+} deposition. SEM images of zinc metal anodes in the c) pristine electrolyte and d) modified electrolyte cells after 1 and 100 cycles at 20 mA cm^{-2} and 5 mAh cm^{-2}. Elemental analysis by energy-dispersive X-ray spectroscopy was difficult due to the close X-ray transition energies of the Ce *M*-edge and the Zn *L*-edge.[21]

electrostatic repulsive force against Zn^{2+}, pushing it away from the protrusions.

As direct evidence, the surfaces of the zinc metal anode after the zinc deposition were examined by scanning electron microscopy (SEM) (Figure 2c,d; Figure S13, Supporting Information). When cycled with the pristine electrolyte, Zn^{2+} is deposited with an uneven distribution (a few μm ≈ several hundred μm) (Figure 2c). In contrast, the modified electrolyte resulted in a uniform distribution and smaller grain sizes upon Zn^{2+} deposition (Figure 2d). These changes well support the improved CE during cycling as well as its suppressed fluctuation by the modified electrolyte (Figure 1e).

The high electric field of Zn^{2+} also causes strong interactions with H_2O, thus forming the hydrated form, $(Zn(H_2O)_6^{2+})$.[22] The coordinated H_2O has weakened O–H bonds because the solvated structure of $Zn(H_2O)_6^{2+}$ induces electron transfer from H_2O to Zn^{2+}. The weakened O–H bonds facilitate the decomposition of H_2O near the zinc metal anode, accelerating the HER.[23] In this regard, our analysis of the modified electrolyte clarifies that the high electron-donating nature of Cl^-, used as an anionic additive, reduces interactions between H_2O and Zn^{2+} by forming a solvation structure with Zn^{2+}, thereby alleviating the HER on the zinc metal anode surface.[24]

The reduced HER activity by the modified electrolyte was directly verified by linear sweep voltammetry (LSV) measurements. The modified electrolyte cell displays a lower HER onset potential (−0.58 V vs SHE) compared to the pristine electrolyte one (−0.53 V vs SHE) (**Figure 3a**). To understand this point in detail, the bonding environments of the prepared electrolytes were investigated by Raman spectroscopy measurements (Figure 3b). The pristine electrolyte exhibits Raman peaks at 170–250 and 390 cm^{-1}, which present the bonding modes of zinc bromide complexes ($[ZnBr_x]^{(2-x)+}$)[25] and zinc hydrate ($[Zn(H_2O)_6]^{2+}$)[24a,b], respectively. A notable difference between the pristine and modified electrolytes is a new broad peak observed at ≈290 cm^{-1}, which is ascribed to the formation of $[Zn(H_2O)_{6-x}Cl_x]^{(2-x)+}$ by the interaction between Cl^- and Zn^{2+}.[22b,24,26] Importantly, as the amount of

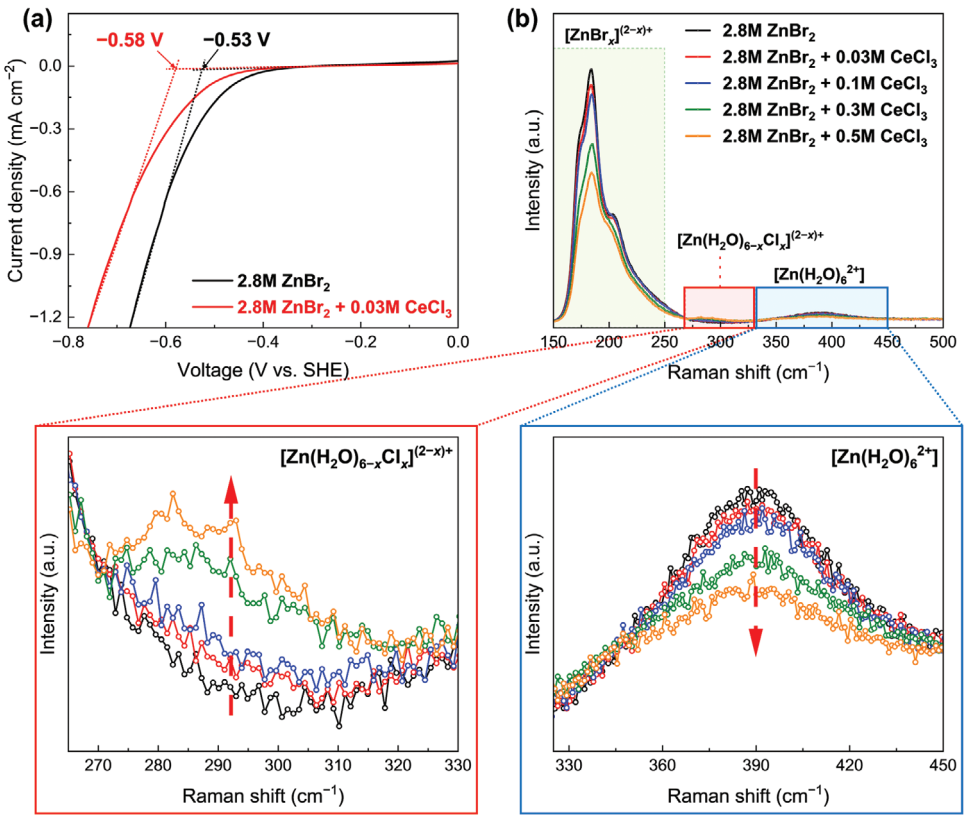

Figure 3. a) *I–V* curves of the pristine electrolyte and modified electrolyte cells. b) Raman spectra of electrolytes containing various amounts of $CeCl_3$ additive.

$CeCl_3$ in the electrolyte increases, this peak increases while the peak from $[Zn(H_2O)_6]^{2+}$ decreases (Figure 3b). These results reveal that Cl^- weakens the interaction between Zn^{2+} and H_2O by participating in bonding within the solvation shells of Zn^{2+}. It is known that during battery operation under the electric fields, solvated zinc ions possessing charge and mobility move closer to the electrode compared to the free water within the electrolyte.[27] Therefore, small changes in solvation structure observed within the electrolyte in this work can significantly influence surface reactions at the electrode surface.

^1H nuclear magnetic resonance analysis (Figures S14,S15, Supporting Information) was further conducted to elaborate on the observed phenomena. For the measurement of pure water in DMSO-d_6, the ^1H peak is observed at 4.30 ppm. When we add 2.8 M $ZnBr_2$, the chemical shift noticeably increases to 4.56 ppm, which indicates a decrease in the electronic density of the protons in H_2O molecules due to the strong coordination between Zn^{2+} and H_2O. In addition, as the $CeCl_3$ additive concentration increases from 0.03 to 0.3 M, the ^1H peaks gradually shift from 4.56 to 4.21 ppm. The lowered ^1H chemical shift directly supports an increase in electronic density due to the addition of Cl^-, clarifying that a part of the coordinated H_2O molecules are released from the zinc ions. These results, once again, reveal the weakened binding between Zn^{2+} and H_2O by Cl^-. On the basis of these results, it can be concluded that the reduced HER activity in the modified electrolyte cell is the result of lowered interactions between H_2O and Zn^{2+} by the high electron-donating Cl^-.

Electrolyte additives have been considered as one of the remedies because the degradation of the zinc metal anode in aqueous batteries typically begins from side reactions between the zinc metal anode and the electrolyte.[28] Our approach, which simultaneously employs both cationic and anionic additives in one compound, is distinctive from previous studies[9,29] that use a single type of additive for the stabilization of the zinc metal anode.

2.3. Large-Scale Cell Verification

The combined cationic and anionic effects of the $CeCl_3$ additive are graphically summarized in **Figure 4a**. On the basis of the stabilized zinc metal reactions by $CeCl_3$ additive, the electrochemical evaluation was expanded to practical non-flow aqueous Zn—Br_2 batteries. It is well-known that aqueous Zn—Br_2 batteries suffer from the severe generation of Br_2 gas during the charging process, which results in significant energy loss during cycling.[30] Additionally, the generated Br_2 at the cathode interacts with Br^- to form highly soluble polybromide anions (Br_3^-, Br_5^-, Br_7^-, etc.). The bromine species (Br_2 and polybromides) easily diffuse from the cathode to the anode, causing unwanted side reactions with the zinc metal anode.[16b,30] Thus, to mitigate these side reactions by the bromine species, a

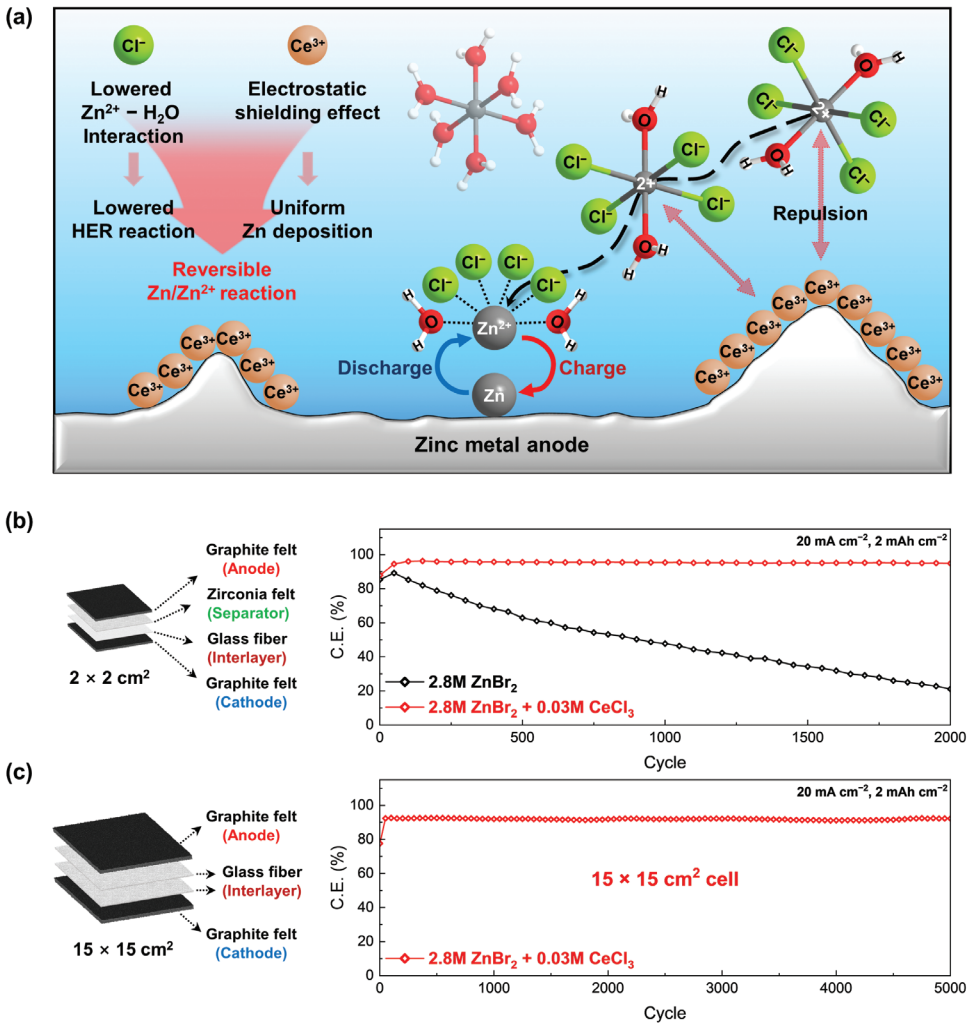

Figure 4. a) Effect of the $CeCl_3$ additive on zinc electrode reaction. Schematic illustrations (left) and cycle performances (right) of the coulombic efficiency of the b) 2 × 2 cm^2 graphite (cathode)/graphite (anode) and c) 15 × 15 cm^2 graphite (cathode)/graphite (anode) cells.

corrosion-resistant graphite[31] and 1-ethylpyridinium bromide (1-EPBr)[9] were used as an anode and a bromine complexing agent (BCA) additive, respectively. Moreover, the thicker (11.9 mm) graphite electrode was employed to minimize the distance between the electrodes, which reduces the ohmic polarization caused by the electrolyte (Figure S17, Supporting Information). The detailed cell configurations are shown in Figure S2b (Supporting Information). Indeed, our preliminary electrochemical tests using non-flow graphite (cathode)/graphite (anode) cells indicate that engaging 1-EPBr as a BCA and thicker graphite results in enhanced CE and reduced overpotential, respectively (Figures S16,S17, Supporting Information).

We first carried out the battery evaluation of the 2 × 2 cm^2 graphite (cathode)/graphite (anode) cells (Figure 4b) with the pristine and modified electrolytes. The stabilized zinc metal reaction by the $CeCl_3$ additive was well reflected in this cell configuration. The modified electrolyte cell retained 94.9% of CE and 70.3% of EE after 2000 cycles (Figure 4b; Figures S18a,S19, Supporting Information). During the entire cycling, the average CE and EE were 95.2% and 74.2%, respectively. After the same number of cycles, however, the pristine electrolyte cell exhibited only 21.1% of CE and 17.4% of EE (Figure 4b; Figures S18b,S19, Supporting Information). Remarkably, the modified electrolyte cell maintained high electrochemical stability even after 5000 cycles (Figure S20, Supporting Information).

Achieving long-term reliable cycling capability in the large-areal battery is also crucial for improving the energy storage performance of aqueous batteries. To this end, the non-flow 15 × 15 cm^2 graphite (cathode)/graphite (anode) cell was fabricated (Figure 4c). A modified electrolyte consisting of 2.8 M $ZnBr_2$ and 0.03 M $CeCl_3$ was employed in this large-scale cell. The cycling performance was evaluated under the same current and an areal capacity as those of 2 × 2 cm^2 cells. This cell delivered a high discharge capacity of 407 mAh after 5000 cycles (Figure S21a, Supporting Information), which corresponds to 92.3% of CE. The average CE during 5000 cycles was 91.8% (Figure 4c). These results demonstrate the practical feasibility of using $CeCl_3$ as an additive in large-scale aqueous Zn—Br_2 batteries. The lowered EE by the large battery area is likely due to the increased overpotential caused by the large interfacial resistance between

the electrode and electrolyte (Figure S21b, Supporting Information). Therefore, investigating battery properties for various cell configurations and their detailed reaction mechanisms would contribute to further enhancing the performance of practical large-scale Zn—Br_2 batteries such as those demonstrated in this study.

3. Conclusion

In conclusion, we introduce $CeCl_3$ as an electrolyte additive to enhance the stability of the zinc electrode in aqueous Zn—Br_2 batteries. The combined effects of Ce^{3+} and Cl^-, which improve the reversibility of Zn plating/stripping and mitigate the HER, respectively, enable the stable operation of non-flow aqueous Zn—Br_2 batteries. Importantly, our study highlights the importance of understanding the different roles of various cationic and anionic additives and utilizing them complementarily to design the electrolyte. This electrolyte design holds promise for application to a range of aqueous batteries that experience multiple simultaneous structural degradations.

4. Experimental Section

Preparation of Electrolytes: Commercial $ZnBr_2$ (Alfa Aesar Co., Inc.) was used as the salt in both the pristine and modified electrolytes. First, 2.8 M of $ZnBr_2$ was dispersed in 8 mL of DI water. $CeCl_3$ (Sigma Aldrich., Inc.) was then added to the pristine electrolyte, and the solution was vigorously stirred for 1 h at room temperature. The $CeCl_3$ concentrations were adjusted to 0, 0.01, 0.03, 0.05, 0.1, 0.3, and 0.5 M. When graphite was used as both the cathode and anode, 0.1 M 1-ethylpyridinium bromide (1-EPBr, Alfa Aesar Co., Inc.) was added to the electrolytes to capture corrosive Br_2 formed by the oxidation of Br^- at the cathode during charging.[9,32]

Characterization: The surface elemental composition of the zinc metal anode before and after the plating process was confirmed using XPS (NEXSA, Thermo Fisher Scientific). The crystal structures of the zinc metal anode were acquired from XRD (SmartLab, Rigaku). The bonding states of aqueous electrolytes were characterized using Raman spectroscopy (LabRAM HR Evolution, Horiba) and nuclear magnetic resonance (Advance Neo 600, Bruker). The morphologies of the surface of the zinc metal anode were monitored by field emission scanning electron microscopy (FE-SEM, JSM-7500F, JEOL). For all the analyses, the cells were disassembled under atmospheric conditions. Separated zinc metal anodes were thoroughly rinsed with DI water to remove any residual electrolytes and additives, and then dried under vacuum conditions.

Battery Assembly: Three types of non-flow aqueous Zn—Br_2 cells were assembled for electrochemical measurements, as shown in Figure S2 (Supporting Information). Graphite (cathode)/Zn (anode) cell was specifically designed to investigate the effects of $CeCl_3$ on the zinc metal anode (Figure S2a, Supporting Information). This cell was fabricated with a 2×2 cm^2 graphite felt (SGL GROUP) (thickness: 4.6 mm) as a cathode, a 2×2 cm^2 Zn foil (Alfa Aesar Co., Inc.) (thickness: 0.62 mm) as an anode, copper plates as current collectors. Graphite bipolar plates and graphite sheets were used to prevent the electrolyte from penetrating into copper plates. After assembling the cell, 8 mL of electrolyte was injected using a vacuum pump.

It is known that the zinc metal anode easily reacts with bromine species generated at the cathode, promoting the corrosion of the zinc metal.[10,16b] To mitigate this effect, a graphite (cathode)/graphite (anode) cell (Figure S2b, Supporting Information) was fabricated. This cell was assembled with two 2×2 cm^2 graphite felt (SGL GROUP) (thickness: 11.9 mm) as electrodes, zirconia felt as a separator, and a glass fiber filter (Whatman) as an interlayer. After assembling the cell, 8 mL of electrolyte was injected using a vacuum pump.

Large-scale graphite (cathode)/graphite (anode) cell was also designed to investigate the practical potential of the $CeCl_3$ additive. The large-scale cell (Figure S2c, Supporting Information) was assembled with two 15×15 cm^2 graphite felts (SGL GROUP) (thickness: 11.9 mm) as electrodes and two glass fiber filters as an interlayer. After assembling the cell, 420 mL of electrolyte was injected under vacuum conditions.

A three-electrode beaker cell was fabricated to investigate the HER reaction at the zinc metal anode. This cell was assembled with a 1×0.5 cm^2 SUS316 foil as the working electrode, a Zn foil (Alfa Aesar Co., Inc.) as the reference electrode, a graphite felt (SGL GROUP) as the counter electrode, and 8 mL of electrolyte. The graphite felts employed in all cells were oxidized at 520 °C for 12 h under ambient air conditions before use to enhance the electrolyte wettability.[33]

Electrochemical Measurements: The cells were cycled galvanostatically at a charging current density of 20 mA cm^{-2} with an areal capacity of 2 mAh cm^{-2} and at a discharging current density of 20 mA cm^{-2} (cut-off voltage: 0.01 V) using a galvanostatic battery cycler (WBCS 3000, Wonatech). Rate capability tests were performed at different discharging current densities (5, 10, 20, 40, 60, and 80 mA cm^{-2}) with a fixed charging current density of 20 mA cm^{-2}. EIS, CV, and LSV were performed using an SP-150e potentiostat (Biologics). EIS data were collected over a frequency range of 10 mHz to 100 kHz with an amplitude of 10 mV. CV data were measured in the voltage range of 0.5 to 2.5 V (vs Zn/Zn^{2+}) at a scan rate of 1 mV s^{-1}. LSV data were measured from 0 to −0.75 V (vs SHE) at a scan rate of 1 mV s^{-1} using a SUS316 as a working electrode, a Zn foil as a reference electrode, and a graphite felt as a counter electrode. All battery evaluations were conducted at room temperature.

Supporting Information

Supporting Information is available from the Wiley Online Library or from the author.

Acknowledgements

This research was supported by the National Research Foundation of Korea (NRF) grant funded by the Ministry of Science and ICT (MSIT) (No. RS-2023-00252931), the 2023 Joint Research Project of Institutes of Science and Technology (G15420), and the Korea Institute of Energy Technology Evaluation and Planning (KETEP) and the Ministry of Trade, Industry & Energy (MOTIE) of the Republic of Korea (No. 20204010600340). The authors sincerely appreciate Prof. Hee-Tak Kim, the professor of the Department of Chemical and Biomolecular Engineering, Korea Advanced Institute of Science and Technology (KAIST), Daejeon, Republic of Korea, for helping to design the non-flow Zn—Br_2 cell platform.

Conflict of Interest

The authors declare no conflict of interest.

Data Availability Statement

The data that support the findings of this study are available from the corresponding author upon reasonable request.

Keywords

aqueous batteries, dendrite, electrolyte additives, hydrogen evolution reaction, Zn anode, Zn—Br_2 batteries

Received: April 3, 2024
Revised: April 26, 2024
Published online: May 7, 2024

[1] a) J. Kalhoff, G. G. Eshetu, D. Bresser, S. Passerini, *ChemSusChem* **2015**, *8*, 2154; b) G. Zubi, R. Dufo-López, M. Carvalho, G. Pasaoglu, *Renewable Sustainable Energy Rev.* **2018**, *89*, 292; c) Z. Zhu, T. Jiang, M. Ali, Y. Meng, Y. Jin, Y. Cui, W. Chen, *Chem. Rev.* **2022**, *122*, 16610.
[2] a) S. Kim, K. W. Nam, S. Lee, W. Cho, J. S. Kim, B. G. Kim, Y. Oshima, J. S. Kim, S. G. Doo, H. Chang, D. Aurbach, J. W. Choi, *Angew. Chem., Int. Ed.* **2015**, *54*, 15094; b) K. W. Nam, S. Kim, S. Lee, M. Salama, I. Shterenberg, Y. Gofer, J. S. Kim, E. Yang, C. S. Park, J. S. Kim, S. S. Lee, W. S. Chang, S. G. Doo, Y. N. Jo, Y. Jung, D. Aurbach, J. W. Choi, *Nano Lett.* **2015**, *15*, 4071; c) J. O. G. Posada, A. J. R. Rennie, S. P. Villar, V. L. Martins, J. Marinaccio, A. Barnes, C. F. Glover, D. A. Worsley, P. J. Hall, *Renewable Sustainable Energy Rev.* **2017**, *68*, 1174; d) P. He, Y. Quan, X. Xu, M. Yan, W. Yang, Q. An, L. He, L. Mai, *Small* **2017**, *13*, 1702551.
[3] S. Biswas, A. Senju, R. Mohr, T. Hodson, N. Karthikeyan, K. W. Knehr, A. G. Hsieh, X. Yang, B. E. Koel, D. A. Steingart, *Energy Environ. Sci.* **2017**, *10*, 114.
[4] Z. Li, M. S. Pan, L. Su, P. C. Tsai, A. F. Badel, J. M. Valle, S. L. Eiler, K. Xiang, F. R. Brushett, Y. M. Chiang, *Joule* **2017**, *1*, 306.
[5] J. H. Lee, Y. Byun, G. H. Jeong, C. Choi, J. Kwen, R. Kim, I. H. Kim, S. O. Kim, H. T. Kim, *Adv. Mater.* **2019**, *31*, 1904524.
[6] J. Zheng, Z. Huang, F. Ming, Y. Zeng, B. Wei, Q. Jiang, Z. Qi, Z. Wang, H. Liang, *Small* **2022**, *18*, 2200006.
[7] R. P. Naresh, P. Ragupathy, M. Ulaganathan, *ACS Appl. Mater. Interfaces* **2021**, *13*, 48110.
[8] a) G. L. Soloveichik, *Chem. Rev.* **2015**, *115*, 11533; b) X. Ke, J. M. Prahl, J. I. D. Alexander, J. S. Wainright, T. A. Zawodzinski, R. F. Savinell, *Chem. Soc. Rev.* **2018**, *47*, 8721; c) H. Jung, J. Lee, J. Park, K. Shin, H. T. Kim, E. Cho, *Small* **2023**, *19*, 2208280.
[9] H. Park, G. Park, S. Kumar, H. Yoon, J. Baek, T. Tamulevičius, S. Tamulevičius, H. J. Kim, *J. Power Sources* **2023**, *580*, 233212.
[10] S. H. Han, S. Kim, H. Y. Lim, S. Park, K. Shin, S. Kim, H. T. Kim, S. K. Kwak, C. Yang, N. S. Choi, *Chem. Eng. J.* **2023**, *464*, 142624.
[11] a) Y. Tian, Y. An, C. Wei, B. Xi, S. Xiong, J. Feng, Y. Qian, *ACS Nano* **2019**, *13*, 11676; b) H. Li, L. Ma, C. Han, Z. Wang, Z. Liu, Z. Tang, C. Zhi, *Nano Energy* **2019**, *62*, 550.
[12] a) Y. P. Deng, R. Liang, G. Jiang, Y. Jiang, A. Yu, Z. Chen, *ACS Energy Lett.* **2020**, *5*, 1665; b) A. Bayaguud, Y. Fu, C. Zhu, *J. Energy Chem.* **2022**, *64*, 246; c) Y. Yang, H. Hua, Z. Lv, M. Zhang, C. Liu, Z. Wen, H. Xie, W. He, J. Zhao, C. C. Li, *Adv. Funct. Mater.* **2023**, *33*, 2212446.
[13] L. Kang, M. Cui, F. Jiang, Y. Gao, H. Luo, J. Liu, W. Liang, C. Zhi, *Adv. Energy Mater.* **2018**, *8*, 1801090.
[14] a) W. Dong, J. L. Shi, T. S. Wang, Y. X. Yin, C. R. Wang, Y. G. Guo, *RSC Adv.* **2018**, *8*, 19157; b) Y. Zeng, X. Zhang, R. Qin, X. Liu, P. Fang, D. Zheng, Y. Tong, X. Lu, *Adv. Mater.* **2019**, *31*, 1903675.
[15] a) L. Cao, D. Li, E. Hu, J. Xu, T. Deng, L. Ma, Y. Wang, X. Q. Yang, C. Wang, *J. Am. Chem. Soc.* **2020**, *142*, 21404; b) X. Guo, Z. Zhang, J. Li, N. Luo, G. L. Chai, T. S. Miller, F. Lai, P. Shearing, D. J. L. Brett, D. Han, Z. Weng, G. He, I. P. Parkin, *ACS Energy Lett.* **2021**, *6*, 395; c) D. Han, Z. Wang, H. Lu, H. Li, C. Cui, Z. Zhang, R. Sun, C. Geng, Q. Liang, X. Guo, Y. Mo, X. Zhi, F. Kang, Z. Weng, Q. H. Yang, *Adv. Energy Mater.* **2022**, *12*, 2102982.
[16] a) L. Gao, Z. Li, Y. Zou, S. Yin, P. Peng, Y. Shao, X. Liang, *iScience* **2020**, *23*, 101348; b) K. Shin, J. H. Lee, J. Heo, H. T. Kim, *Curr. Opin. Electrochem.* **2022**, *32*, 100898.
[17] a) Y. Jin, K. S. Han, Y. Shao, M. L. Sushko, J. Xiao, H. Pan, J. Liu, *Adv. Funct. Mater.* **2020**, *30*, 2003932; b) C. Lin, Y. Liu, X. Zhang, X. Miao, Y. Chen, S. Chen, Y. Zhang, *J. Power Sources* **2022**, *549*, 232078; c) B. Niu, Z. Li, D. Luo, X. Ma, Q. Yang, Y. E. Liu, X. Yu, X. He, Y. Qiao, X. Wang, *Energy Environ. Sci.* **2023**, *16*, 1662.
[18] J. Heo, K. Shin, H. T. Kim, *Adv. Sci.* **2022**, *9*, 2204908.
[19] a) X. Guan, A. Wang, S. Liu, G. Li, F. Liang, Y. W. Yang, X. Liu, J. Luo, *Small* **2018**, *14*, 1801423; b) P. Zou, R. Zhang, L. Yao, J. Qin, K. Kisslinger, H. Zhuang, H. L. Xin, *Adv. Energy Mater.* **2021**, *11*, 2100982.
[20] M. C. Wu, T. S. Zhao, L. Wei, H. R. Jiang, R. H. Zhang, *J. Power Sources* **2018**, *384*, 232.
[21] R. D. Deslattes, E. G. Kessler, P. Indelicato, L. de Billy, E. Lindroth, J. Anton, *Rev. Mod. Phys.* **2003**, *75*, 35.
[22] a) H. Yang, Z. Chang, Y. Qiao, H. Deng, X. Mu, P. He, H. Zhou, *Angew. Chem., Int. Ed.* **2020**, *59*, 9377; b) Q. Zhang, Y. Ma, Y. Lu, L. Li, F. Wan, K. Zhang, J. Chen, *Nat. Commun.* **2020**, *11*, 4463; c) X. Wang, Z. Zhang, B. Xi, W. Chen, Y. Jia, J. Feng, S. Xiong, *ACS Nano* **2021**, *15*, 9244.
[23] a) F. Wang, O. Borodin, T. Gao, X. Fan, W. Sun, F. Han, A. Faraone, J. A. Dura, K. Xu, C. Wang, *Nat. Mater.* **2018**, *17*, 543; b) L. Cao, D. Li, F. A. Soto, V. Ponce, B. Zhang, L. Ma, T. Deng, J. M. Seminario, E. Hu, X. Q. Yang, P. B. Balbuena, C. Wang, *Angew. Chem., Int. Ed.* **2021**, *60*, 18845.
[24] a) C. Zhang, J. Holoubek, X. Wu, A. Daniyar, L. Zhu, C. Chen, D. P. Leonard, I. A. Rodríguez-Pérez, J. X. Jiang, C. Fang, X. Ji, *ChemComm* **2018**, *54*, 14097; b) C. Y. Chen, K. Matsumoto, K. Kubota, R. Hagiwara, Q. Xu, *Adv. Energy Mater.* **2019**, *9*, 1900196; c) Q. Zhang, Y. Ma, Y. Lu, X. Zhou, L. Lin, L. Li, Z. Yan, Q. Zhao, K. Zhang, J. Chen, *Angew. Chem., Int. Ed.* **2021**, *60*, 23357.
[25] M. M. Yang, D. A. Crerar, D. E. Irish, *J. Solution Chem.* **1988**, *17*, 751.
[26] G. P. Rajarathnam, T. K. Ellis, A. P. Adams, B. Soltani, R. Zhou, P. J. Cullen, A. M. Vassallo, *J. Electrochem. Soc.* **2021**, *168*, 070522.
[27] a) B. Li, X. Zhang, T. Wang, Z. He, B. Lu, S. Liang, J. Zhou, *Nano-Micro Lett.* **2021**, *14*, 6; b) Z. Cao, X. Zhu, D. Xu, P. Dong, M. O. L. Chee, X. Li, K. Zhu, M. Ye, J. Shen, *Energy Storage Mater.* **2021**, *36*, 132; c) H. Yan, S. Li, J. Zhong, B. Li, *Nano-Micro Lett.* **2023**, *16*, 15.
[28] K. E. K. Sun, T. K. A. Hoang, T. N. L. Doan, Y. Yu, X. Zhu, Y. Tian, P. Chen, *ACS Appl. Mater. Interfaces* **2017**, *9*, 9681.
[29] a) M. C. Wu, T. S. Zhao, H. R. Jiang, Y. K. Zeng, Y. X. Ren, *J. Power Sources* **2017**, *355*, 62; b) Z. Liu, J. Ren, F. Wang, X. Liu, Q. Zhang, J. Liu, P. Kaghazchi, D. Ma, Z. Chi, L. Wang, *ACS Appl. Mater. Interfaces* **2021**, *13*, 27085; c) K. Ouyang, D. Ma, N. Zhao, Y. Wang, M. Yang, H. Mi, L. Sun, C. He, P. Zhang, *Adv. Funct. Mater.* **2022**, *32*, 2109749; d) Y. Dai, C. Zhang, W. Zhang, L. Cui, C. Ye, X. Hong, J. Li, R. Chen, W. Zong, X. Gao, J. Zhu, P. Jiang, Q. An, D. J. L. Brett, I. P. Parkin, G. He, L. Mai, *Angew. Chem., Int. Ed.* **2023**, *62*, 202301192.
[30] W. Wu, S. Xu, Z. Lin, L. Lin, R. He, X. Sun, *Energy Storage Mater.* **2022**, *49*, 11.
[31] C. Wang, Q. Lai, P. Xu, D. Zheng, X. Li, H. Zhang, *Adv. Mater.* **2017**, *29*, 1605815.
[32] D. J. Eustace, *J. Electrochem. Soc.* **1980**, *127*, 528.
[33] Q. Ye, Y. J. Zhang, P. Cheng, Z. Shao, *Int. J. Heat Mass Transfer* **2020**, *156*, 119911.